PCB-Based Magnetic Integration and Design Optimization for Three-Phase LLC

Rimon Gadelrab, *Student Member, IEEE*, and Fred C. Lee, *Life Fellow, IEEE*

***Abstract*—The *LLC* converter is the most efficient topology in server and telecom applications. Furthermore, three interleaved *LLC* converters have been shown to yield efficiency advantages at power levels of several kilowatts. The magnetic components of a multiphase *LLC*, on the other hand, are complex, laborious, and difficult to build cost-effectively. To solve these issues, a high-frequency GaN-based three-phase *LLC* converter is used in this research. With GaN working at 500 kHz, all magnetic components, including six inductors and six transformers, can be housed in a single structure, while all magnetic windings are accommodated in a four-layer PCB with 3 oz. of copper. Furthermore, electromagnetic interference can be improved by virtue of three-phase by 20 dB and an additional two layers are added to gain an additional 20–30 dB reduction from a low frequency up to 30 MHz. The proposed construction is simple and economically mass-producible. A 6 kW 400V/48V 3-phase prototype is implemented, with a peak efficiency of over 99% and a power density of 1000 W/in3 (61 kW/L)**

***Index Terms*—Data center, electromagnetic interference (EMI) shielding, integrated magnetics, *LLC* resonant converter, planar transformer, server, three-phase *LLC*, telecom power supply.**

I. Introduction

FOR a typical configuration, the AC/12 V power supply unit for data center architecture will have a power output of 1 kW [1]. Power supplies for data center architecture with 48 V buses, such as the one shown in Fig. 1(b), and. power supplies for telecom equipment, on the other hand, are frequently designed to have an output of 3–5 kW [2] to accommodate the expected high electrical energy consumption as depicted in Fig. 1(a) [3]. Full-bridge design, as opposed to half-bridge configuration, may be used for the primary side of the converter [4]. It will lead to more power being output but also more current and voltage ripples being produced. Multiple types of two-phase interleaved *LLC* converters have been described in [4], [5], and [6], but in order to accomplish current sharing, all two-phase interleaved *LLC* converters need extra switches, components, and a control algorithm. This raises the cost of the system and lowers its efficiency.

Manuscript received 9 January 2023; revised 16 April 2023; accepted 8 June 2023. Date of publication 13 June 2023; date of current version 22 September 2023. This work was supported by Power Management Consortium in the Center for Power Electronics Systems (CPES), Virginia Tech. Recommended for publication by Associate Editor H. Krishnamoorthy. *(Corresponding author: Rimon Gadelrab.)*

The authors are with the Center for Power Electronics Systems, Virginia Tech., Blacksburg, VA 24061 USA (e-mail: rimongg@vt.edu; fclee@vt.edu).

Color versions of one or more figures in this article are available at https://doi.org/10.1109/TPEL.2023.3285652.

Digital Object Identifier 10.1109/TPEL.2023.3285652

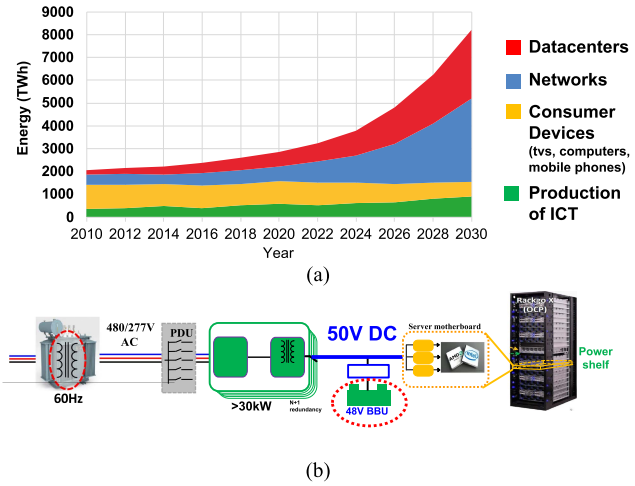

Fig. 1. Data center power architecture with narrow bus voltage range. (a) IT electric power consumption trend. (b) Forty-eight volt power architectures with narrow voltage range.

However, three-phase *LLC* can be used to improve the magnetic design of the *LLC* resonant converter by taking advantage of the advantages of a three-phase system in terms of magnetic integration and loss, electromagnetic interference (EMI) performance, and smaller output voltage ripples [7], [8], [9], [10], [11].

For a 6–9 kW power supply, roughly six transformers are required for the dc–dc stage to handle the high-output current. A three-phase *LLC* is proposed for the dc–dc stage of a 6–9 kW power supply. The proposed solution can achieve high density and high efficiency with a fully automated solution due to the utilization of the PCB winding to integrate all the magnetics into PCB.

With GaN devices running at hundreds of kilohertz have been designed for different applications and significantly improved power density has been demonstrated [12], [13], [14]. However, these applications have low output voltage and smaller magnetic size and the eddy loss inside the core is negligible.

Therefore, for higher output voltage by increasing bus voltage in the data center from 12 to 48 V as shown in Fig. 1, magnetic size is getting bigger, therefore, it is preferred to optimize the switching frequency and the core shape as demonstrated in [15], [16], and [17].

In this article, a novel three-*LLC* topology proposed with an improved magnetic integration and a novel SRs' technique is proposed to significantly reduce the termination loss and

asymmetry among three-phase rectifier termination loops. It also focuses on the magnetics integration, design process, shielding effectiveness, and light-load improvement of a three-phase *LLC* for the dc–dc stage. A 6-kW prototype is demonstrated to verify all the demonstrated analyses.

II. Review 3-kW PCB-Based Magnetics Design

A 3 kW *LLC* with the highest efficiency of 99% has been presented in [17] where a matrix transformer of three elemental transformers has been used to handle the 3-kW output as depicted in Fig. 2(a). In this article, impact of eddy loss in the ferrite material has been discussed with proposed solutions to reduce this loss including the impact of the core-legs arrangement, core shape, and winding shape to optimize the core losses. To extend this concept to higher power, following the design optimization in [17], different number of transformers have been designed and compared at the same footprint as shown in Fig. 2(b), where three transformers give the best balance between core loss and winding loss while maintaining minimum total loss. Fig. 2(c) shows a 3-kW prototype of three-transformer, which can achieve a peak efficiency of 99%, to achieve high-density, thermal vias is utilized to eliminate the need of heatsink to achieve low profile solution. Therefore, the optimum power per PCB-based transformer is around 1–1.5 kW can be concluded as concluded in Fig. 3. Hence, for a 6 kW or higher, six transformers are required as shown in Fig. 4. However, for six transformers, three phase can add additional benefits from the magnetic integration point of view utilizing the benefit of flux cancellation for a three-phase transformer leading to a more compact, simplified, and efficient structure, in addition to other benefits as it will be discussed in the following sections.

This article focuses on the magnetics integration, design process, shielding effectiveness, and light load improvement of three-phase *LLC* for dc–dc stage. A 6-kW prototype is demonstrated to verify all the analyses done.

III. Proposed Magnetic Integration of Three-Phase *LLC*

Fig. 4 shows the proposed three-phase *LLC* topology with six transformers and three resonant inductors for 6 kW 400-48 V. The demonstrated single-phase magnetic design for *LLC* resonant converter in [17] could well be readily expanded to a greater power level by utilizing three magnetic cells each house two transformers (as depicted in Fig. 5). A resonant inductor is required to fulfill the hold-up time requirements [18]. For a six-transformer structure, adding additional three resonant inductors will make the structure. Fig. 4 proposes three-phase *LLC* topology complex and is not cost-effective; therefore, in this section, a proposed integrated leakage inductance is demonstrated to create a leakage inductance within the transformers' windings and legs without adding additional winding or legs for the inductor.

However, for a perfect interleaved winding as shown in Fig. 6(a), there will be no leakage inductance created because the flux created by the primary winding ($N_{p1}i_p$ or $N_{p2}i_p$) for each transformer (for instance T_1 or T_2) will be canceled by the

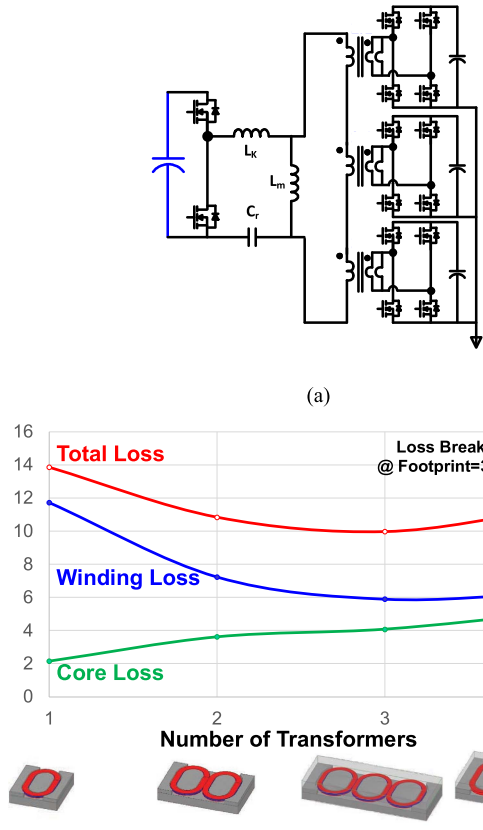

Fig. 2. PCB-based transformer power limit. (a) Matrix transformer schematic. (b) Optimum power per transformer. (c) Three-transformer prototype.

flux created by the secondary winding ($N_{s1}i_{s1}$ or $N_{s2}i_{s2}$) for the same transformer:

Since $N_{p1} = N_{p2}$, $N_{s1} = N_{s2}$ and the primary winding is in series, and hence $i_{s1} = i_{s2}$; therefore

$$N_{p1}\, i_p = N_{p2}\ \ i_p = N_{s1}\ \ i_{s1} = N_{s2}\, i_{s2}. \tag{1}$$

To create a leakage inductance, the balance between primary and secondary side winding has to be broken [20], therefore, one

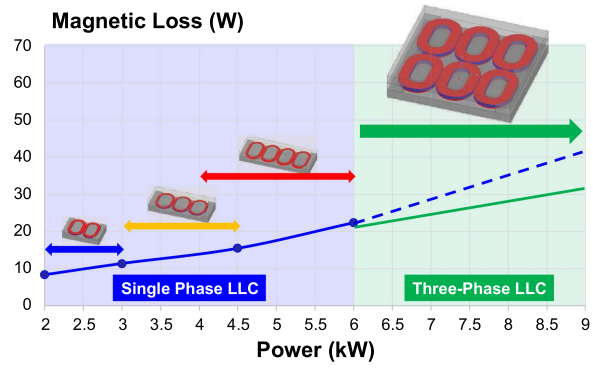

Fig. 3. Modular design approach for PCB-based magnetics.

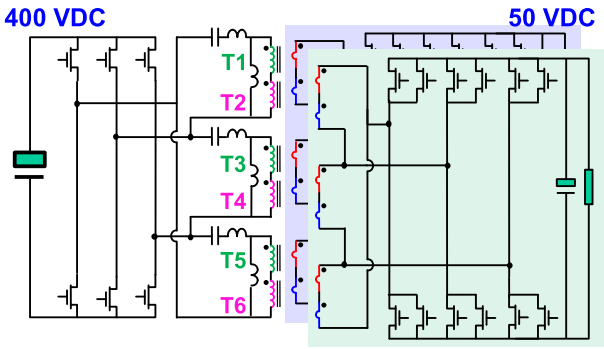

Fig. 4. Proposed three-phase *LLC* topology.

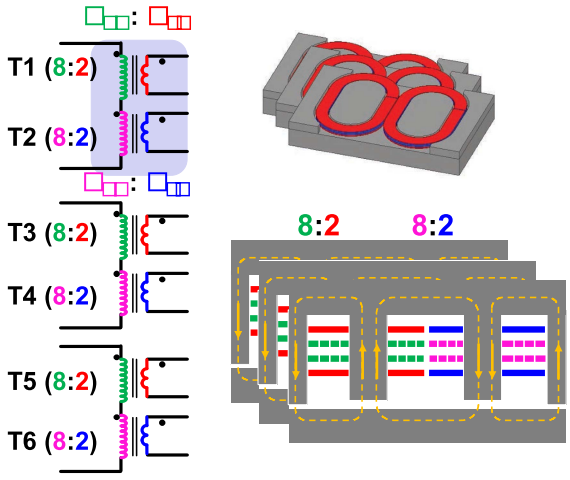

Fig. 5. Integration of two transformers into one UI-core.

primary turn from the transformer T_2 is moved to the transformer T_1 and to ensure the current sharing among parallel secondary winding (N_{s1} and N_{s2}), the secondary is reconnected in series first then in parallel as shown in Fig. 6(b); therefore

$$N_{p1}i_p \neq N_{p2}i_p \neq N_{s1}i_s \neq N_{s2}i_s. \tag{2}$$

And a leakage inductance has been created. From the reluctance model, the magnetizing inductance and leakage inductance equations can be derived as following under the assumption of zero air gap for the side legs and hence: (see the appendix for

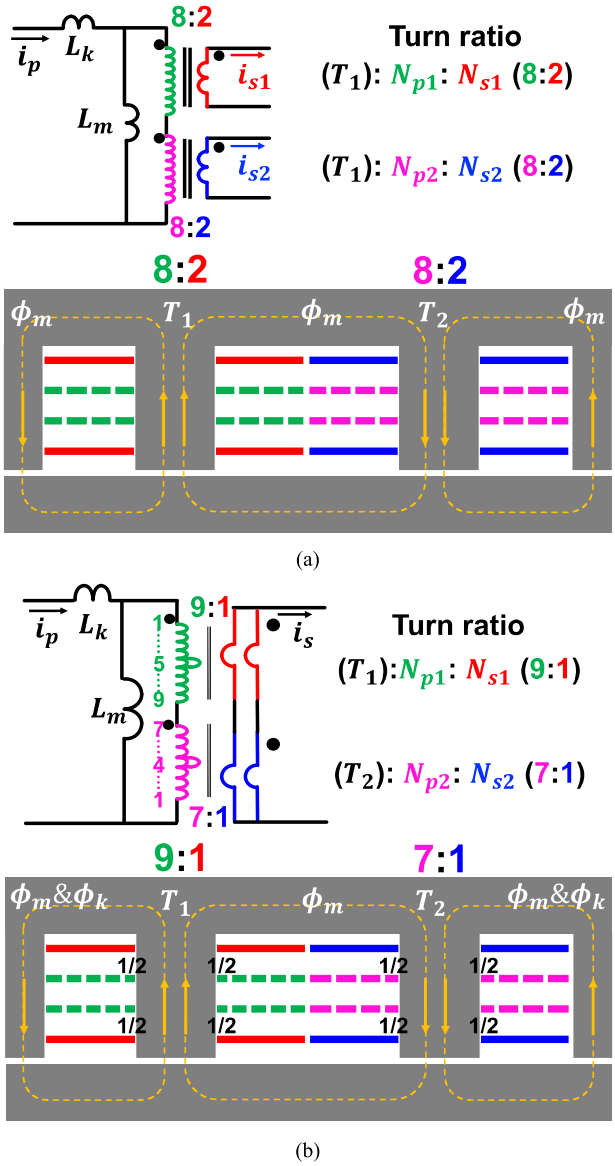

Fig. 6. Integration of built-in leakage inductance. (a) Perfect interleaved winding with no leakage. (b) Unbalanced primary winding to create leakage inductance.

detailed derivation)

$$L_m = \frac{2N_{p1}N_{p2}}{R_{g1}} \tag{3}$$

$$L_k = \frac{(N_{p1} - N_{p2})^2}{R_{g1}} \tag{4}$$

$$L_n = \frac{L_m}{L_k} = \frac{(N_{p1} - N_{p2})^2}{2N_{p1}N_{p2}}. \tag{5}$$

Equations (3)–(5) show that the created leakage inductance can be controlled by the unbalance of primary winding across the two transformers of each phase.

To utilize the benefit of three-phase flux cancellation, the three EI-cores are integrated together into one entity as shown in Fig. 7(a), this allows the three-phase flux to add together in the

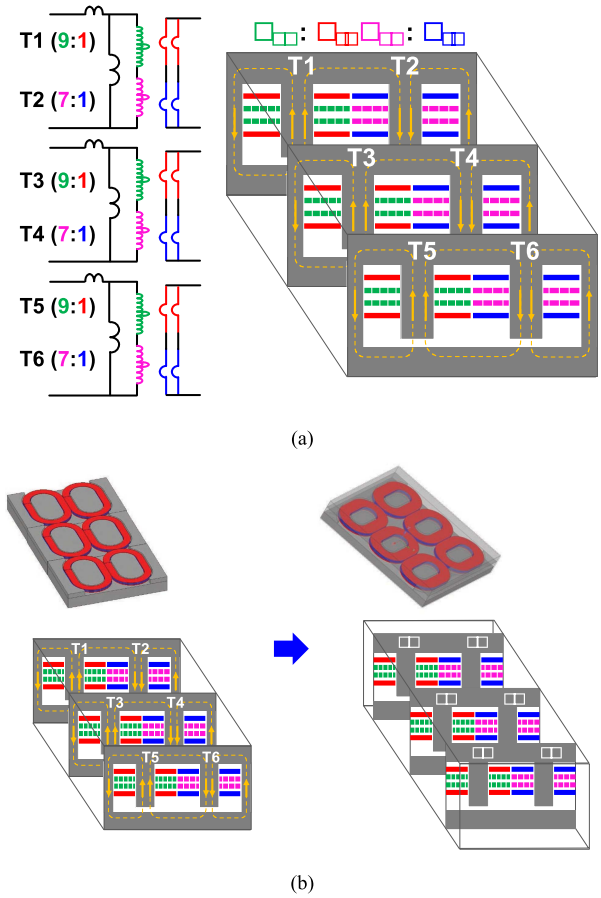

Fig. 7. Proposed magnetic integration with built-in leakage inductance. (a) Based on three EI-cores integrated. (b) Further improved magnetic integration.

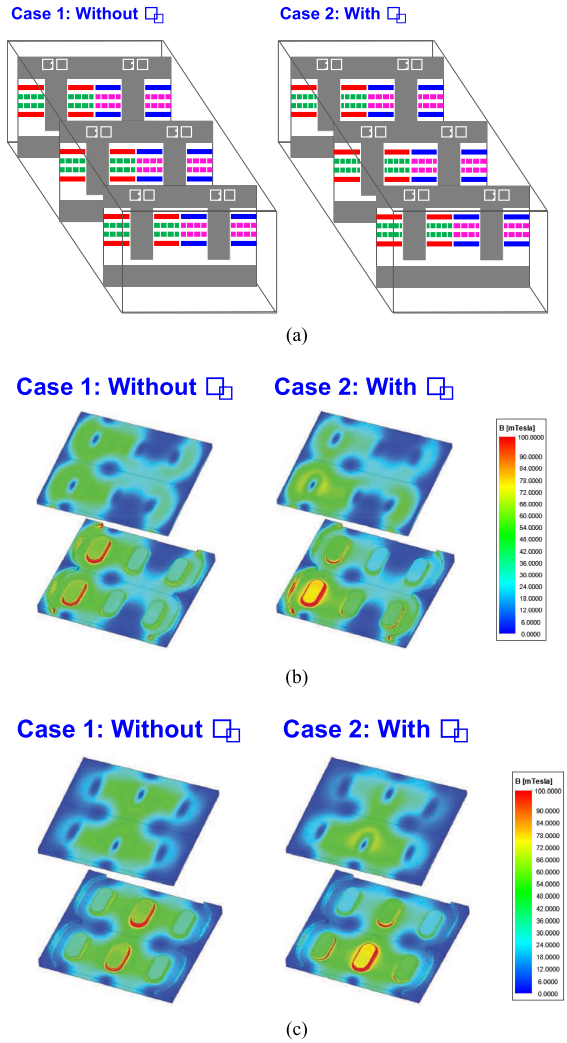

Fig. 8. Effect of integrating built-in leakage inductance (based on 500 kHz and 180 mm^2 cross-sectional area for the middle legs). (a) Impact of integrating leakage inductance on winding arrangement. (b) 3D simulation at the time instant when the flux density of phase one (left two legs) is at its peak. (c) 3D simulation at the time instant when the flux density of phase two (middle two legs) is at its peak.

side legs which will reduce the flux in the side legs and plates due to the three-phase flux cancellation property. Therefore, the magnetic structure can be taken one step forward to simply the structure and hence further reduce the core loss and core size as shown in Fig. 7(b) by rearranging the side legs and save 20% of the footprint. In addition, rearranging the side legs as proposed can yield extra benefits compared to the structure in [17].

1) Uniform flux distribution in the plates and around the legs.
2) Symmetrical structure among the three-phase transformer by providing symmetrical paths for the flux of each phase.
3) Smaller core loss due to better flux distribution.
4) Smaller tolerance for the leakage inductance and magnetizing inductance values among the three phases to ensure symmetry.

Fig. 8(a) shows the impact of integrating leakage inductance on the transformer winding structure by moving one turn from one transformer leg to the other which will slightly break the transformer perfect interleaving. The cost of adding this leakage flux in the core is shown in Fig. 8(b) and (c), 3D simulation is used to evaluate the core loss for both cases, with leakage inductance and without leakage inductance. The results show a 3.9 W core loss for case 1 (without leakage inductance) and 4.7 W for case 2 (with leakage inductance).

Therefore, the integration of six leakage inductors only adds 0.8 W or 20% additional core loss without the need to add more winding and/or leg which will save additional loss and footprint.

However, removing the side legs will create unsymmetric paths for the three-phase flux, phase 1 and phase 3 are symmetric, but phase 2's flux path is different. This difference will create asymmetric magnetizing inductances (L_{m1}, L_{m2}, and L_{m3}) and leakage inductances. In addition, the side legs will help for better flux distribution in the plates as shown in Fig. 8 and hence reduce the core loss.

Compared to three-single-phase interleaved with discrete magnetic structure as shown in Fig. 9 and magnetic integration in [19], the proposed magnetic integration has minimum core loss with better symmetry among the three-phase compared to [19] as summarized in Table I, the comparison is done using 3D Ansys simulation under the same conditions.

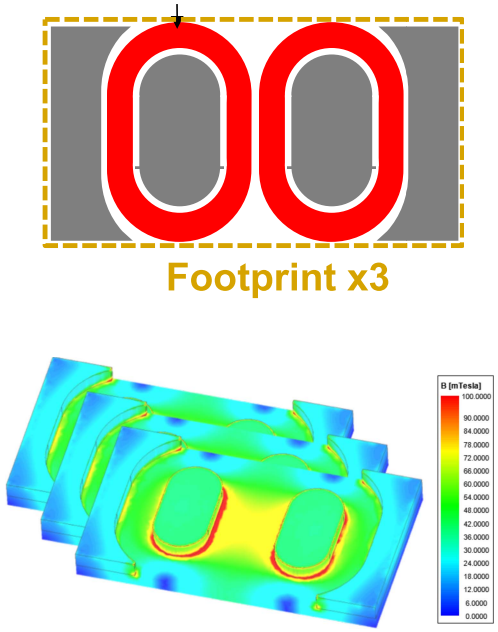

Fig. 9. Discrete three-phase *LLC*.

TABLE I
SUMMARIZED BENEFITS OF THE PROPOSED MAGNETIC STRUCTURE

	Core Loss	Lm1	Lm2	Lm3
[19]	6.9 W	74 μH	80.2 μH	74 μH
Proposed	4.7 W	74 μH	76 μH	74 μH
Discrete	8 W	74 μH	74 μH	74 μH

IV. DESIGN OF 6 KW 400V/48V THREE-PHASE *LLC*

In this section, the magnetic design of the proposed structure is presented. However, the switching frequency *fs* is selected 500 kHz and the number of the elemental transformers is two transformer per phase to follow the established modular design of 1 kW per transformer.

A. Optimization Process

1) Identify the Design Variables: In this step, the design variables are identified based on the magnetic dimensions as shown in Fig. 10, and the design variables can be identified as *r, c,* L_{rect}, P_{vc}.

Middle legs cross-sectional area

$$A_{e1} = \pi r^2 + 2rL_{\text{rect}}. \tag{6}$$

Outer legs cross-sectional area

$$A_{e2} = A_{e1} = bW. \tag{7}$$

Plate thickness

$$h_{\text{plate}} = \frac{\text{A}_{\text{e1}}}{W}, \text{suchthat } B_{m_{\text{plate}}} = B_{m_{\text{leg}}}. \tag{8}$$

$$\text{Footprint} := 2\left(2r + 2c + L_{\text{rect}}\right)\left(6r + 6c + 2b\right). \tag{9}$$

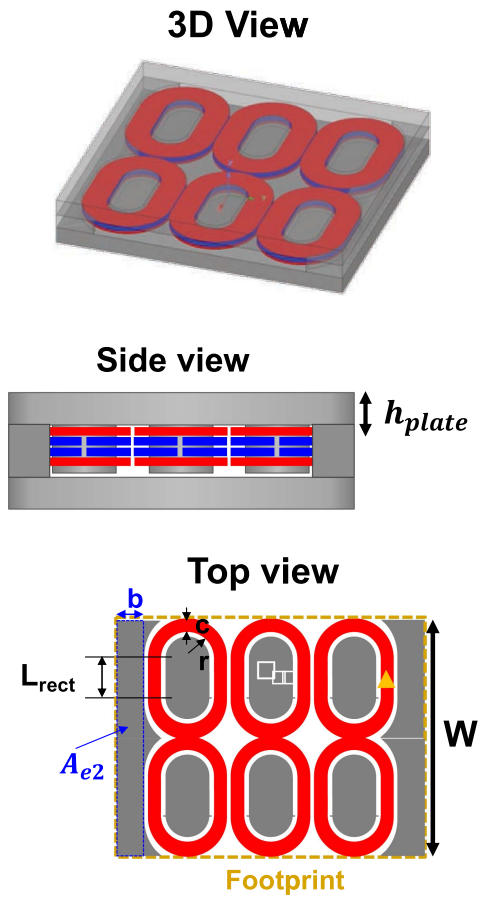

Fig. 10. Magnetic structure dimensions.

2) Set $P_{VC} = 200\,\text{kW/m}^3$*:* Based on the P_{VC}, B_m can be calculated and hence the core cross sections area as follows:

$$B_m = \frac{V_o}{4f_S A_{e1}} = 68\text{ mT} \tag{10}$$

- $A_{e1} = 180\text{ mm}^2$
- $A_{e2} = A_{e1} = 180\text{ mm}^2$

3) Reduce Design Variables to r *and* c*:* For a given cross-sectional area, L_{rect} and *b* can be expressed as a function of *r* and *c*.

From (5)

$$L_{\text{rect}} = \frac{\boldsymbol{A_{e1} - \pi r^2}}{\boldsymbol{2r}}. \tag{11}$$

From (9)

$$\text{b} = \frac{0.5\boldsymbol{A_{e1}r}}{\boldsymbol{A_{e1} - \pi r^2 + 4r^2 + 4cr}}. \tag{12}$$

Therefore, magnetic loss, core loss, and winding loss can be calculated as a function of *r* and *c*.

4) Calculate Core Loss and Winding Loss: Finite element analysis (FEA) is utilized to account for nonuniform flux/current distribution as shown in Fig. 11.

1) Winding loss using 2D FEA simulation; winding thickness = 3 oz, skin depth @ 500 kHz, plotted in Fig. 11(a).
2) Core loss using 3D FEA simulation, plotted in Fig. 11(b).

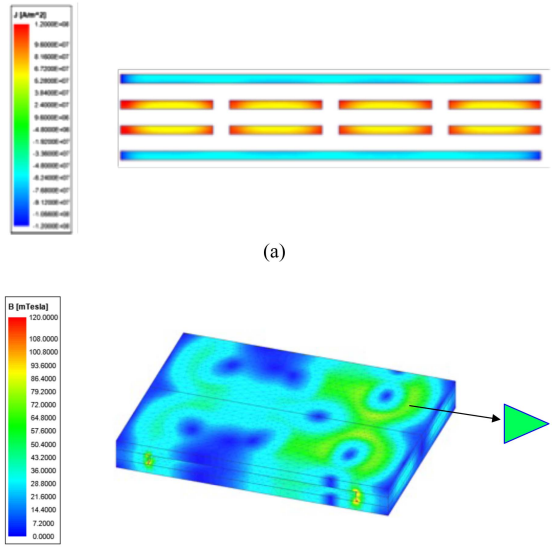

(a)

(b)

Fig. 11. Magnetic loss model. (a) Winding loss model using 2D FEA. (b) Core loss model using 3D FEA.

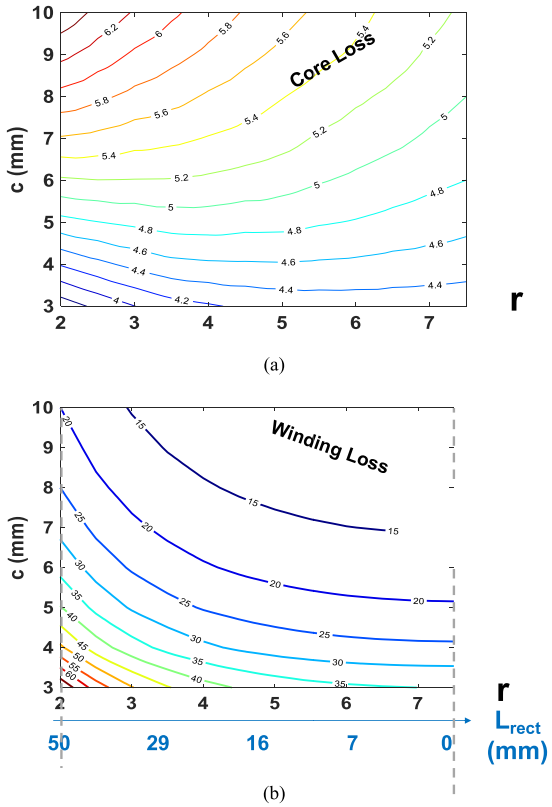

(a)

(b)

Fig. 12. Magnetic loss calculation. (a) Core loss. (b) Winding loss.

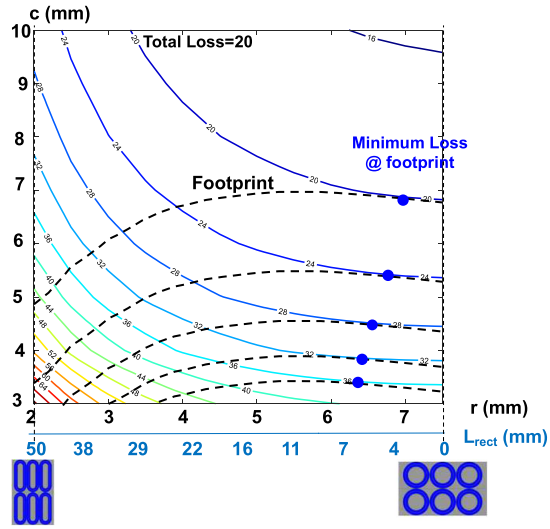

Fig. 13. Transformer total loss versus core radius r and winding width c.

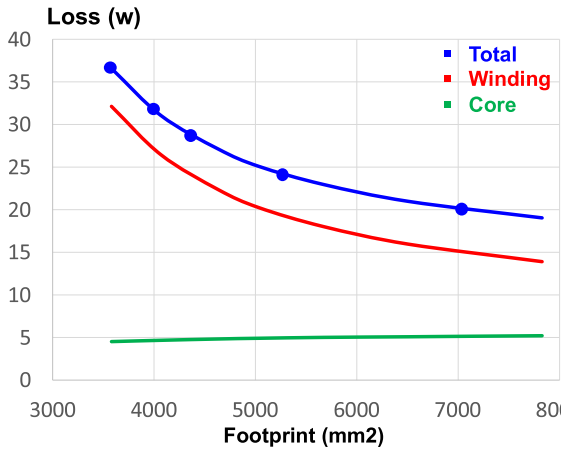

Fig. 14. Minimum loss versus footprint for $P_{VC} = 200 \frac{\text{kW}}{\text{m}^3}$.

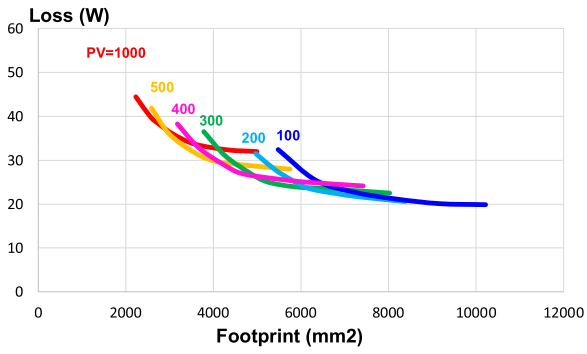

Fig. 15. Minimum loss versus footprint for different.

5) Trade-Between Total Loss Versus Footprint: As a result, the total magnetic loss as well as the footprint can be computed as a function of the core's radius r and the winding's width c, as illustrated in Fig. 12. And the total versus footprint is given in Fig. 13. Fig. 14 is a plot of the least magnetic loss versus the footprint for the proposed magnetic integration structure. This data was obtained after all of the optimal design points for a specific footprint range had been swept.

6) Sweep $P_{VC} = 100$–$1000\,kW/m^3$: In this step P_{VC} is swept and the steps from 2 to 5 have been repeated and the results are plotted in Fig. 15. The design region is selected between 4000 and 8000 mm^2 to achieve low loss with high density.

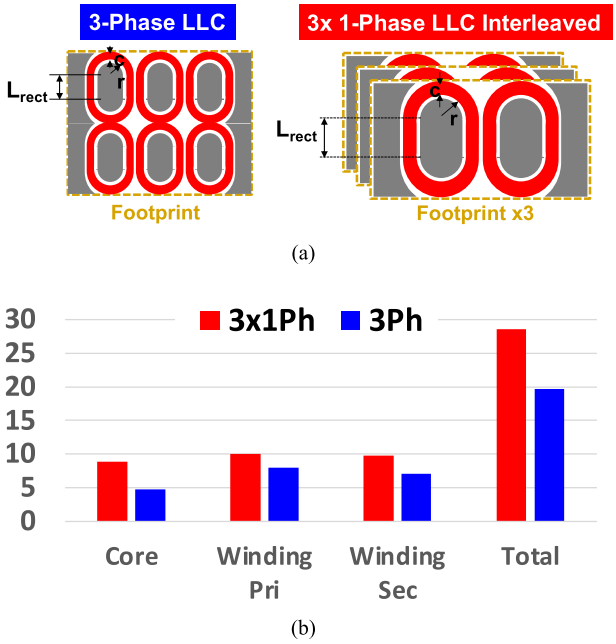

Fig. 16. Three-phase *LLC* versus three-single phase LLC. (a) Magnetic structure. (b) Magnetic loss comparison.

TABLE II
DESIGN DIMENSIONS

Dimensions	Three Phase	Three single phase
r	6.5 mm	7 mm
c	7 mm	6 mm
L_{rect}	7.5 mm	10 mm
Plate thickness	3.3 mm	5 mm

The design steps are repeated for three-single phase interleaved and the same footprint is chosen to compare the three-single phase *LLC* and three-phase *LLC* as shown in Fig. 16(a) and the magnetic dimensions are listed in Table II, and magnetic loss are shown in Fig. 16(b).

Three-phase *LLC* has less both core and winding loss, in addition due to the smaller volt-second applied to the transformer, refer to the transformer voltage waveform in the phase shedding section, the three-phase has:

1) 46% core loss reduction;
2) 24% winding loss;
3) 34% Plate thickness reduction;
4) 30% higher power density.

V. PROPOSED DISTRIBUTED SRS FOR BETTER TERMINATION

For single-phase *LLC* with a matrix transformer, the secondary side consists of multiple sets of outputs to handle the high current. Each output set has its dedicated rectifier, either a center-tapped rectifier or a full-bridge rectifier, as discussed in [17]. Therefore, the secondary side termination loop is very short and symmetrical across all the outsets' rectifiers. However, in the case of the three-phase *LLC*, there are interconnections between the output rectifiers as shown in Fig. 18(a), which introduces some challenges in the termination loop.

For the three-phase *LLC*, each half-bridge rectifier on the secondary sides is shared among two phases, for instance, the red half-bridge in Fig. 17(a) is shared between phase 1 and phase 3, therefore from the termination loop drawings, the red and cyan loops, phase 1 and phase 3 termination loops are unsymmetrical with different leakage inductance among the

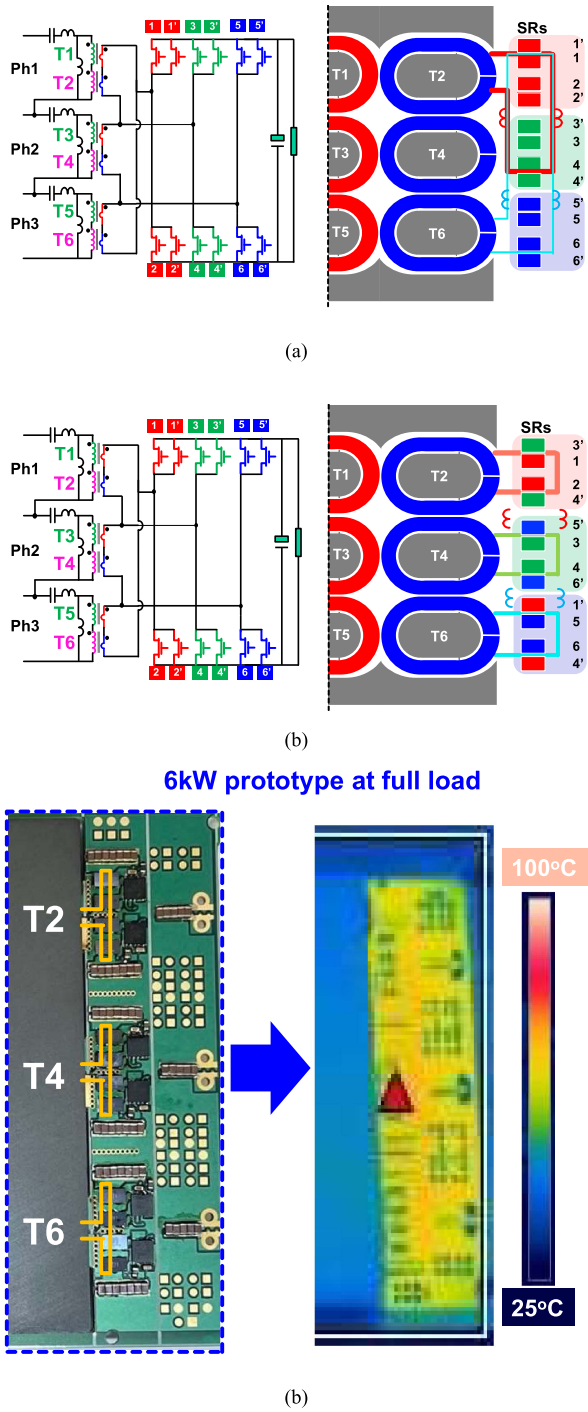

Fig. 17. SRs termination layout. (a) Conventional termination for three-phase LLC. (b) Proposed distributed SRs termination. (c) Thermal verification of SRs current sharing.

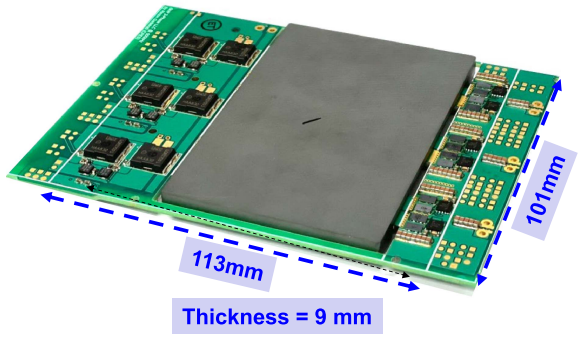

(a)

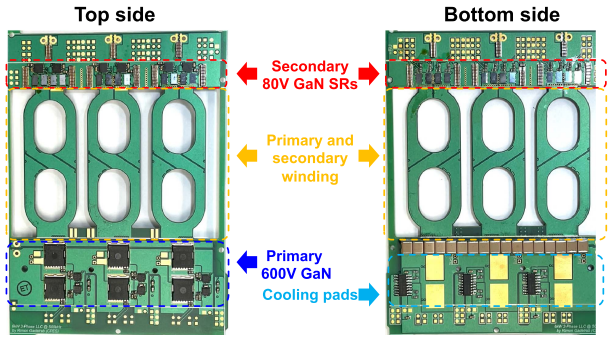

(b)

Fig. 18. Hardware 6 kW 400 V/48 V prototype. (a) 3D View of prototype with the core assembled. (b) Top and bottom view of the PCB with magnetic core.

two phases. In addition, the long termination loop at this high switching frequency will generate tremendous termination loop loss due to parasitic inductances. For high output current, two parallel SRs are required to handle the output current as shown in Fig. 17(a). These parallel SRs will reduce the device conduction loss but termination is still the same for conventional way of paralleling the SRs.

Fig. 17(b) shows the proposed distributed SRs, where the parallel SRs are relocated in a way to minimize the termination loop as well as single-phase *LLC* with negligible parasitic inductances and to ensure the symmetry among all the three-phase termination loops. Fig. 17(c) provides the thermal performance of the proposed distributed SRs which verify a good current sharing among the parallel SRs.

VI. Prototype and Experimental Results

The 500 kHz 6 kW 400 V/48 V *LLC* converter prototype with the proposed integrated transformers and resonant inductors is shown in Fig. 18. An output power of 6 kW at such a dimension is equivalent to a power density of around 1000 W/inch^3 and the prototype specifications are given in Table III.

In Fig. 19, we can see the experimental waveforms for both full- and light-load scenarios. Here, it is shown that ZVS may be attained for both the primary side and secondary side devices in both full-load and light-load scenarios. In addition, since

TABLE III
Specifications of the Proposed Three-Phase *LLC* Converter

Component	Parameters
Resonant Frequency	500 kHz
Dead Time	100 ns
Transformer turns ratio	16:2
Primary devices	PGA26E07BA
Secondary devices	EPC 2029
Primary Driver	Si8273GBD
Secondary Drivers	LM5113
Resonant Capacitor	33.8 nF
Resonant Inductance	3 μH
Magnetizing Inductance	72 μH

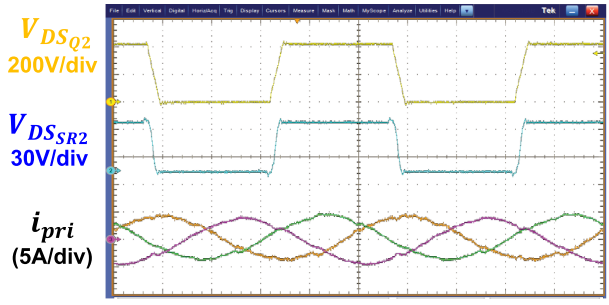

(a)

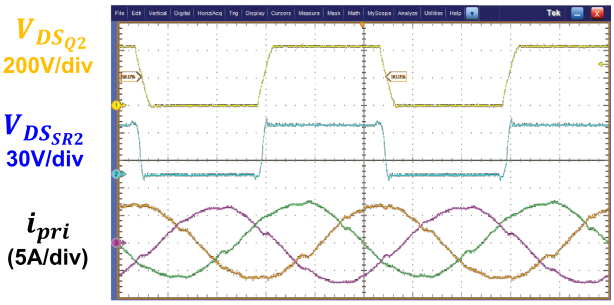

(b)

Fig. 19. Testing waveforms. (a) Light load. (b) Heavy load.

secondary leakage is kept to a minimal, the V_{dsSR} does not exhibit any ringing.

A. Tested Efficiency

Fig. 20 shows the three-phase *LLC* in comparison with paralleling two of the prototypes with three elemental transformers presented in [17]. The proposed three-phase *LLC* converter with a built resonant inductor for regulation has a peak efficiency of 99.11%, a full-load efficiency of 98.6%, and a light-load (10% load) efficiency of 96.48%, which clearly highlights the benefits of three-phase *LLC* versus three interleaved *LLC*. The efficiency of the proposed *LLC* converter is much higher than the state-of-the-art high-frequency *LLC* converters and almost the same efficiency as state-of-art three-phase *LLC* with way better and simplified magnetic structure and at least five times higher power density.

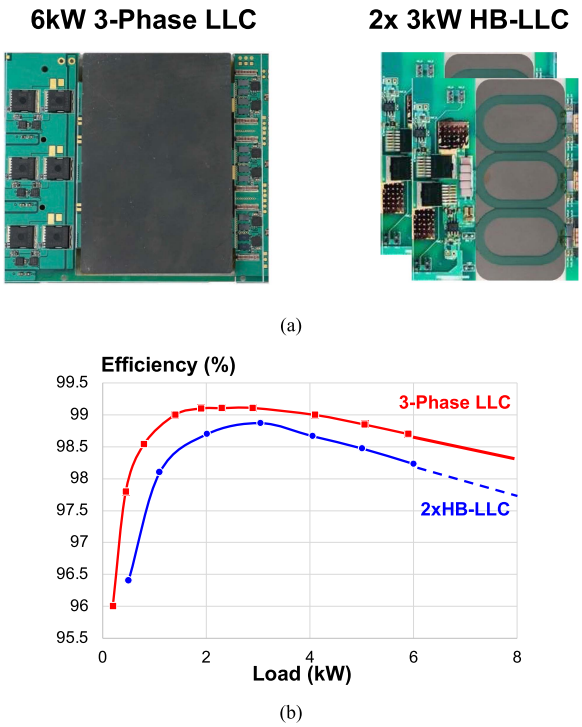

Fig. 20. Six kilowatt three-phase *LLC* versus 2 × 3 kW single-phase LLC. (a) Hardware prototypes. (b) Tested efficiency.

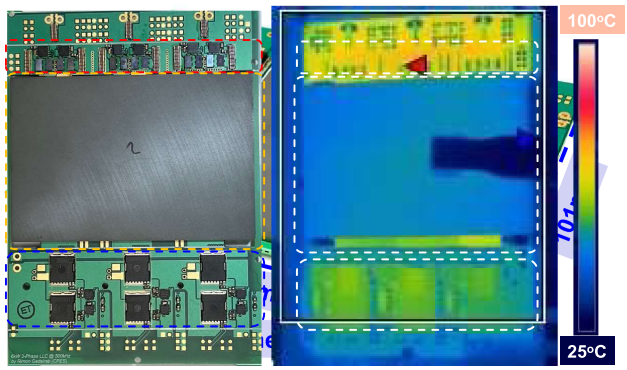

Fig. 21. Thermal performance at full load (6 kW).

Full load, 25 degrees Celsius ambient temperature, and 200 linear feet per minute fan speed were used to conduct thermal tests on the proposed *LLC* converter, the results of which are shown in Fig. 21. Secondary devices may go up to 90 degree Celsius hotter. There is no risk of overheating with any of the two primary and secondary devices. Both the primary side and secondary side FETs operate within the acceptable temperature range.

The use of planar magnetic cores, as opposed to the more traditional, cylindrical magnetic cores, contributes to the suggested design's superior thermal performance. This is because the high-efficiency design incorporates both a high surface area to volume ratio and a high-efficiency design. In comparison to traditional wire-wound components, the planar magnetics are superior in their ability to dissipate heat, which results in far lower temperature increases.

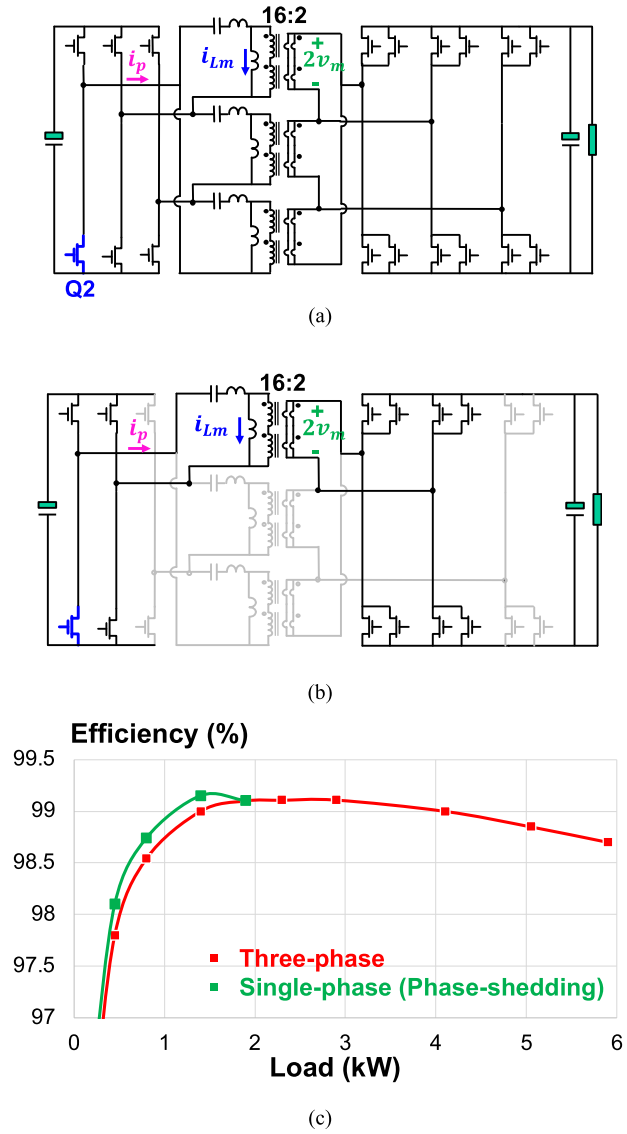

Fig. 22. Phase shedding for light load efficiency improvements. (a) Three-phase operation. (b) Single-phase operation. (c) Tested efficiency.

B. Phase Shedding for Improving the Light Load Efficiency

At light load condition, the dominant loss is load-independent loss which is the device switching loss, especially for high switching frequency design, and the magnetic core loss which only depends on the volt-second; therefore, it depends on the output voltage, however, it does not depend on the output current. Hence, to further improve the light load efficiency, two phases can be shut off and only one phase provides the power to the load as shown in Fig. 22 [20].

From Fig. 23, the volt-second can be derived under the assumption of ignoring the commutation time as follows:

$$\text{Volt}-\text{second}\ |_{3-\text{Phase}} = \int_0^{T_s/3} V_o = \frac{1}{3} V_o T_s \qquad (13)$$

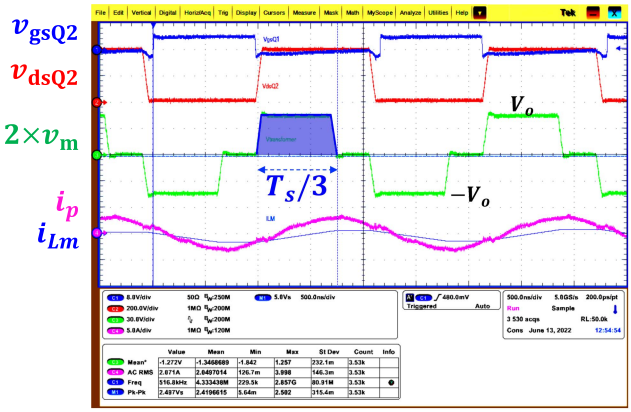

(a)

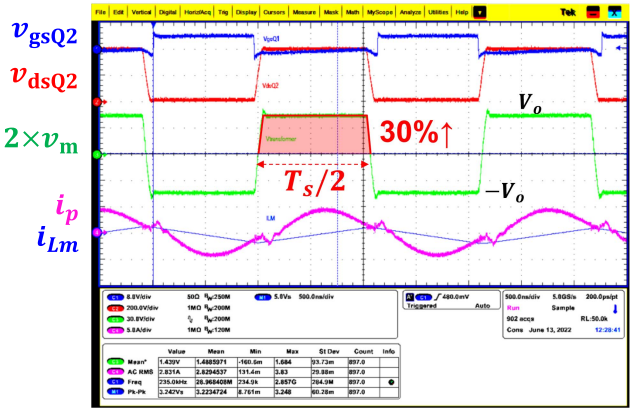

(b)

Fig. 23. Light-load waveforms and phase shedding. (a) Three-phase operation. (b) Single-phase operation.

TABLE IV
BENEFIT OF PHASE SHEDDING

Loss (W)	Three-Phase operation	Single phase operation
Core Loss	4.8	3.2
Primary Side switching loss	2.6	1.7
Primary Side conduction loss	1.1	1.4

$$\text{Volt}-\text{second}\ |_{3-\text{Phase}} = \int_0^{T_s/3} V_o = \frac{1}{3} V_o T_s. \tag{14}$$

Hence, single-phase operation increases the transformer volt-second by 33.33%. Table IV shows the benefit of phase shedding in reducing the core loss and switching loss, however, the reduction of core loss is not very significant due to the 33% increase of the volt-second applied to the transformer by changing from three-phase operation to a single-phase operation as shown in Fig. 23.

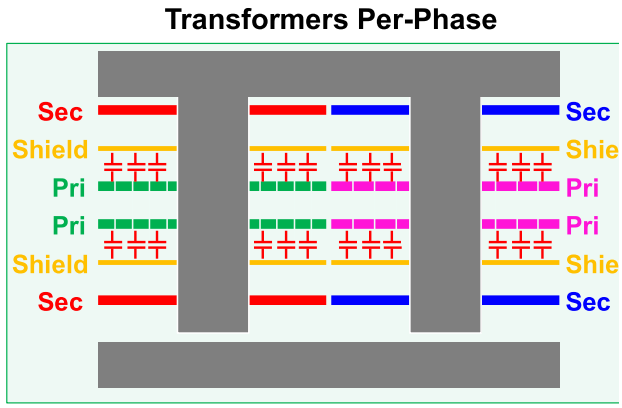

Fig. 24. Implementation of shielding to block the CM current.

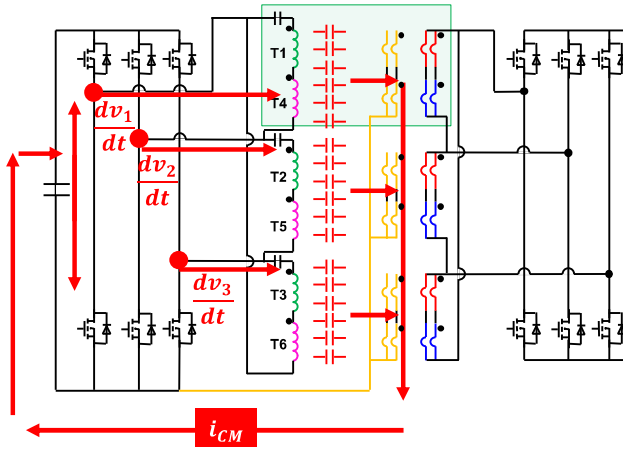

Fig. 25. CM current path with the shielding layers.

VII. SHIELDING AND EMI PERFORMANCE

For the PCB magnetics, there are large overlapping areas between the primary side and secondary side windings which will create a large inter-winding capacitance, as shown in Fig. 24, and hence large CM currents will flow from the primary side to the secondary. To solve this issue, two layer shieldings are inserted between the primary winding and secondary winding to block the CM current from flowing into the secondary and provide an alternative path for the CM current to return to the primary ground as shown in Fig. 25 [21].

Fig. 26 shows the benefit of the added shielding layers. A total of 20–28 dB reduction has been achieved from the fundamental frequency up to 40 MHz which demonstrates the effectiveness of shielding layers up to very high frequencies. In addition to the EMI benefits from the shielding, three-phase *LLC* has naturally better EMI performance due to the cancellation effect of the harmonics as follows: theoretically

CM current $(i_{\text{CM}}) \approx C_{\text{EPC}}(\frac{d_{v1}}{dt} + \frac{d_{v2}}{dt} + \frac{d_{v3}}{dt}) \approx 0\ \forall$ harmonics except third order and its multiples.

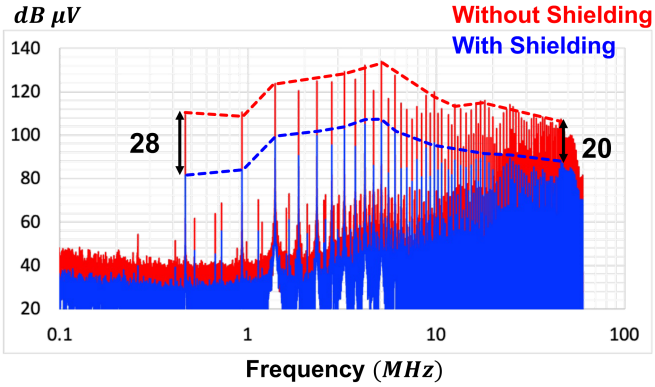

Fig. 26. Tested EMI (benefit of the added shielding layers).

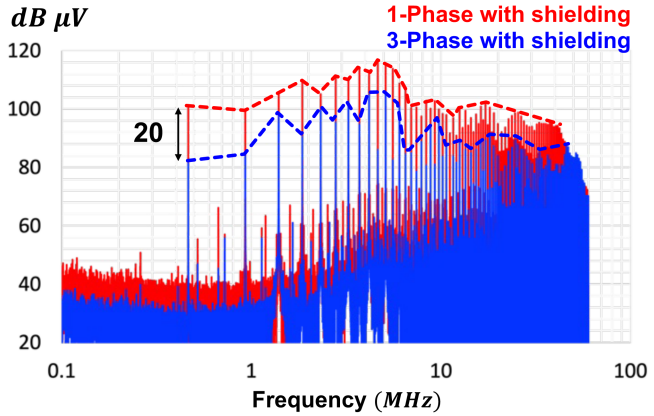

Fig. 27. Tested EMI (benefit of three-phase *LLC*).

Fig. 27 shows the tested EMI for three-phase *LLC* and single-phase *LLC* with shielding, hence, 20 dB reduction for fundamental frequency and better overall EMI performance >8 dB for up to 40 MHz.

The single-phase EMI testing is done on the same prototype of the three-phase *LLC* with phase shedding to ensure the same conditions among both cases with similar interwinding capacitance, hence, the difference between the tested EMI for both cases is from the circuit difference.

VIII. Conclusion

Since the *LLC* converter is very efficient and can handle a lot of power, it is widely used as a dc/dc converter in data center and telecommunications equipment. Additional advantages of a three-phase interleaved *LLC* converter include higher output power, lower input and output current ripples, and automated current sharing across phases. However, there are a lot of magnetic parts in a three-phase *LLC* converter, which causes problems. Reducing the size of the magnetics is made possible by increasing the switching frequency using GaN devices to several hundreds of kilohertz. Six inductors and six transformers are combined into a single magnetic core in this unique magnetic construction proposed in this research. In addition, a four-layer PCB winding may be used for all the magnetics at switching

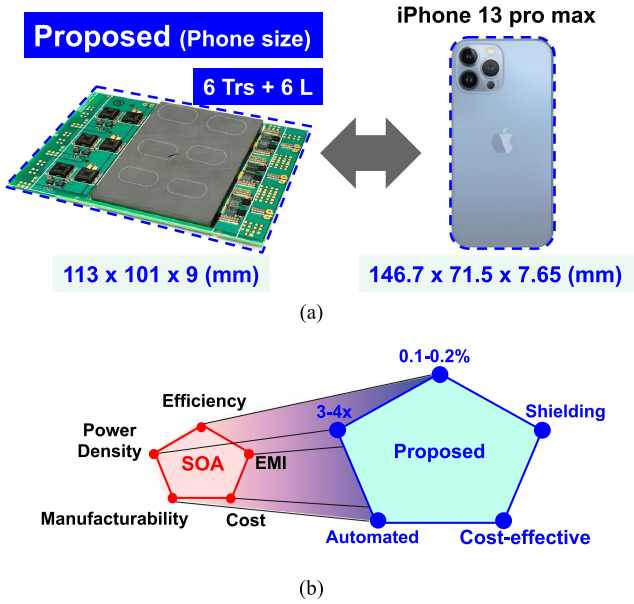

Fig. 28. Influence of GaN-PCB-based integrated magnetics. (a) Proposed solution. (b) Proposed aspects of improvements compared to the SOA.

frequencies of less than 500 kHz, and extra two-layer shielding can be included to lower CM noise. Both the main and secondary sides of the proposed three-phase *LLC* converter use delta-connected resonant networks. The procedure for optimizing the design of the suggested magnetic structure is also presented.

Based on Fig. 28, it is clear that an efficient, power-dense, and easily manufacturable GaN-based three-phase interleaved *LLC* converter with integrated magnetics is suggested. This study makes a significant academic advance by allowing us to develop a converter with more than 10 times the switching frequency and power density of current practice utilizing silicon devices while retaining a greater efficiency. The suggested magnetic structure is used to create a 500 kHz 6 kW, 400 V/48 V three-phase *LLC* converter with a peak efficiency of 99.1% and a power density of 1000 W/inch^3.

Appendix

Fig. 29(a) shows the proposed integrated magnetics for six elemental transformers and six resonant inductors, and Fig. 29(b) shows the corresponding reluctance model. Under the assumption that the core reluctance is negligible, and the airgaps reluctances are dominant, therefore, the reluctance model can be simplified. Based on the reluctance model, the flux in each leg can be calculated as follows:

$$\varphi_1 = \frac{(5N_{p1} - N_{p2})\,R_{g1} + 6N_{p1}R_{g2}}{6R_{g1}^2 + 9R_{g1}R_{g2}}\, i_{p1}$$

$$- \frac{(N_{p1} + N_{p2})\,R_{g1} + 3N_{p1}R_{g2}}{6R_{g1}^2 + 9R_{g1}R_{g2}}\, (i_{p2+i_{p3}})$$

$$+ \frac{(5N_{s1} - N_{s2})\,R_{g1} + 6N_{s1}R_{g2}}{6R_{g1}^2 + 9R_{g1}R_{g2}}\, i_{s1}$$

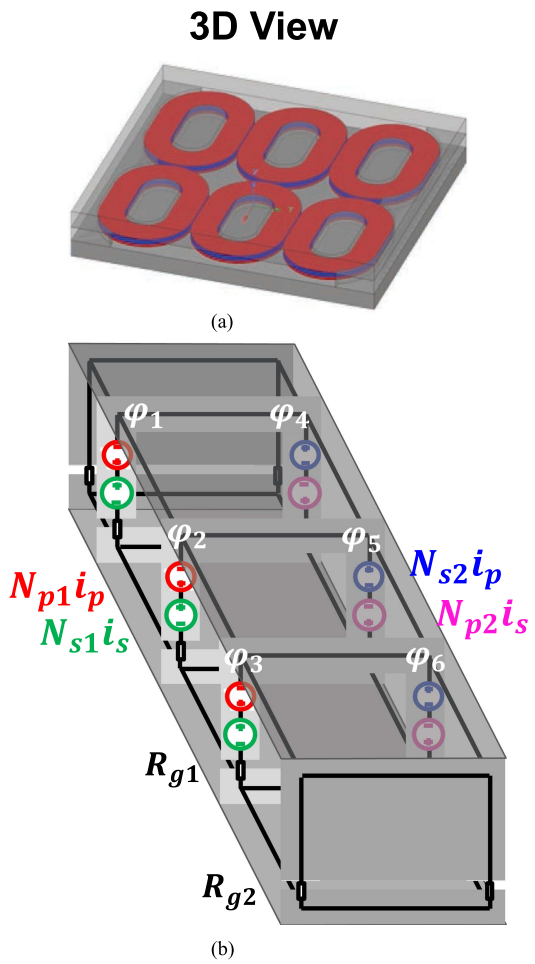

Fig. 29. Integrated magnetics of one phase (two transformers and two resonant inductors). (a) Integrated two elemental transformers. (b) Reluctance model of two elemental transformers.

$$- \frac{(N_{s1}+N_{s2})\,R_{g1}+3N_{s1}R_{g2}}{6R_{g1}^2+9R_{g1}R_{g2}}\,(i_{s2}+i_{s3}) \tag{15}$$

$$\varphi_4 = \frac{(5N_{p2}-N_{p1})\,R_{g1}+6N_{p2}R_{g2}}{6R_{g1}^2+9R_{g1}R_{g2}}\,i_{p1} - \frac{(N_{p1}+N_{p2})\,R_{g1}+3N_{p1}R_{g2}}{6R_{g1}^2+9R_{g1}R_{g2}}\,(i_{p2}+i_{p3}) + \frac{(5N_{s2}-N_{s1})\,R_{g1}+6N_{s2}R_{g2}}{6R_{g1}^2+9R_{g1}R_{g2}}\,i_{s1} - \frac{(N_{s1}+N_{s2})\,R_{g1}+3N_{s1}R_{g2}}{6R_{g1}^2+9R_{g1}R_{g2}}\,(i_{s2}+i_{s3})\,. \tag{16}$$

From symmetry

$$\varphi_2 = \varphi_1 = \varphi_3 \tag{17}$$

$$\varphi_4 = \varphi_5 = \varphi_6. \tag{18}$$

From Faraday's Law

$$L = N\frac{d\varphi}{di} \tag{19}$$

$$L_{\text{self}} = \left(\frac{N_{p1}d\varphi_1}{di_p} - \frac{N_{p2}d\varphi_4}{di_p}\right)\Big|_{i_s=0} = \frac{R_{g1}\left(5N_{p1}^2+2N_{p1}N_{p2}+5N_{p2}\right)+R_{g2}\,\left(6N_{p1}^2+6N_{p2}^2\right)}{6R_{g1}^2+9R_{g1}R_{g2}} \tag{20}$$

$$M = \left(\frac{N_{p1}d\varphi_1}{di_s} - \frac{N_{p2}d\varphi_2}{di_s}\right)\Big|_{i_{p1}=0} = -\frac{R_{g1}N_{p1}(N_{s2}-5N_{s1})-R_{g1}N_{p2}(N_{s1}-5N_{s2})-R_{g2}(6N_{p1}N_{s1}-6N_{p2}N_{s2})}{6R_{g1}^2+9R_{g1}R_{g2}}. \tag{21}$$

Under the assumptions

$$N_{s1} = N_{s2} = 1 \tag{22}$$

$$R_{g2} = 0 \tag{23}$$

$$L_m = -M\,\frac{N_{p1}+N_{p2}}{N_{s1}+N_{s2}} = \frac{2N_{p1}N_{p2}}{R_{g1}} \tag{24}$$

$$L_k = L_{\text{self}} - L_m = \frac{(N_{p1}-N_{p2})^2}{R_{g1}} \tag{25}$$

$$L_n = \frac{L_m}{L_k} = \frac{(N_{p1}-N_{p2})^2}{2N_{p1}N_{p2}}\,. \tag{26}$$

From (26), the ratio between the magnetizing inductance to the leakage inductance is a function of the difference between the primary winding of the left leg (N_{p1}) and primary winding of the right leg (N_{p2}), therefore, for a symmetrical primary winding, the controllable leakage inductance cannot be created as shown in Fig. 29(b), therefore we have to break the symmetry of the primary winding to create a controllable leakage inductance.

REFERENCES

[1] F. C. Lee, Q. Li, Z. Liu, Y. Yang, C. Fei, and M. Mu, "Application of GaN devices for 1 kW server power supply with integrated magnetics," *CPSS Trans. Power Electron. Appl.*, vol. 1, no. 1, pp. 3–12, Dec. 2016, doi: 10.24295/CPSSTPEA.2016.00002.

[2] J. Biela, U. Badstuebner, and J. W. Kolar, "Design of a 5-kW, 1-U, 10-kW/dm- resonant DC–DC converter for telecom applications," *IEEE Trans Power Electron.*, vol. 24, no. 7, pp. 1701–1710, Jul. 2009, doi: 10.1109/TPEL.2009.2014377.

[3] N. Jones, "How to stop data centres from gobbling up the world's electricity," *Nature*, vol. 561, no. 7722, pp. 163–166, Sep. 2018, doi: 10.1038/D41586-018-06610-Y.

[4] Z. Hu, Y. Qiu, L. Wang, and Y.-F. Liu, "An interleaved LLC resonant converter operating at constant switching frequency," *IEEE Trans Power Electron.*, vol. 29, no. 6, pp. 2931–2943, Jun. 2014, doi: 10.1109/TPEL.2013.2273939.

[5] Z. Hu, Y. Qiu, Y.-F. Liu, and P. C. Sen, "A control strategy and design method for interleaved LLC converters operating at variable switching frequency," *IEEE Trans Power Electron.*, vol. 29, no. 8, pp. 4426–4437, Aug. 2014, doi: 10.1109/TPEL.2014.2300165.

[6] H. Wu, X. Zhan, and Y. Xing, "Interleaved LLC resonant converter with hybrid rectifier and variable-frequency plus phase-shift control for wide output voltage range applications," *IEEE Trans Power Electron.*, vol. 32, no. 6, pp. 4246–4257, Jun. 2017, doi: 10.1109/TPEL.2016.2602545.

[7] J. Cao, X. Zhang, P. Rao, S. Zhou, F. Zhou, and Q. Zhang, "Design of three-phase delta-delta LLC resonant converter," in *Proc. IEEE Veh. Power Propulsion Conf.*, 2020, pp. 1–5, doi: 10.1109/VPPC49601.2020.9330918.

[8] R. Gadelrab, F. C. Lee, and Q. Li, "Three-phase interleaved LLC resonant converter with integrated planar magnetics for telecom and server application," in *Proc. IEEE Conf. Appl. Power Electron. Conf. Expo.*, 2020, pp. 512–519, doi: 10.1109/APEC39645.2020.9124392.

[9] C. Fei, R. Gadelrab, Q. Li, and F. C. Lee, "High-frequency three-phase interleaved LLC resonant converter with GaN devices and integrated planar magnetics," *IEEE J. Emerg. Sel. Topics Power Electron.*, vol. 7, no. 2, pp. 653–663, Jun. 2019, doi: 10.1109/JESTPE.2019.2891317.

[10] Y. Nakakohara, H. Otake, T. M. Evans, T. Yoshida, M. Tsuruya, and K. Nakahara, "Three-phase LLC series resonant DC/DC converter using SiC MOSFETs to realize high-voltage and high-frequency operation," *IEEE Trans. Ind. Electron.*, vol. 63, no. 4, pp. 2103–2110, Apr. 2016, doi: 10.1109/TIE.2015.2499721.

[11] E. Orietti, P. Mattavelli, G. Spiazzi, C. Adragna, and G. Gattavari, "Current sharing in three-phase LLC interleaved resonant converter," in *Proc. IEEE Energy Convers. Congr. Expo.*, 2009, pp. 1145–1152, doi: 10.1109/ECCE.2009.5316510.

[12] D. Huang, S. Ji, and F. C. Lee, "LLC resonant converter with matrix transformer," in *Proc. IEEE Appl. Power Electron. Conf. Expo.*, 2014, pp. 1118–1125. doi: 10.1109/APEC.2014.6803447.

[13] M. Mu and F. C. Lee, "Design and optimization of a 380v-12v high-frequency, high-current LLC converter with GaN devices and planar matrix transformers," *IEEE J. Emerg. Sel. Topics Power Electron.*, vol. 4, no. 3, pp. 854–862, Sep. 2016, doi: 10.1109/JESTPE.2016.2586964.

[14] D. Reusch and F. C. Lee, "High frequency bus converter with low loss integrated matrix transformer," in *Proc. IEEE 27th Annu. Appl. Power Electron. Conf. Expo.*, 2012, pp. 1392–1397, doi: 10.1109/APEC.2012.6166002.

[15] A. Nabih, R. Gadelrab, Q. Li, and F. C. Lee, "Dimensional effects of core loss and design considerations for high frequency magnetics," in *Proc. IEEE Energy Convers. Congr. Expo.*, 2021, pp. 5488–5495, doi: 10.1109/ECCE47101.2021.9595465.

[16] A. Nabih, R. Gadelrab, P. R. Prakash, Q. Li, and F. C. Lee, "High power density 1 MHz 3 kW 400 V-48 v LLC converter for datacenters with improved core loss and termination Loss," in *Proc. IEEE Appl. Power Electron. Conf. Expo.*, 2021, pp. 304–309, doi: 10.1109/APEC42165.2021.9487232.

[17] R. Gadelrab, A. Nabih, F. C. Lee, and Q. Li, "LLC resonant converter with 99% efficiency for data center server," in *Proc. IEEE Appl. Power Electron. Conf. Expo.*, 2021, pp. 310–319, doi: 10.1109/APEC42165.2021.9487423.

[18] S. Badha and G. Bernacchia, "OCPV3 BBU : Ideal battery pack configuration and highly efficient /responsive BiDir DCDC converter," 2020. [Online]. Available: https://www.opencompute.org/documents/open-rack-v3-bbu-module-spec-1-3-pdf-1

[19] C. Fei, B. Li, F. C. Lee, Q. Li, and H. Wu, "Interleaved converters with integrated magnetics," 2020. Accessed: Oct. 15, 2021. [Online]. Available: www.huawei.com

[20] F. Jin, A. Nabih, Q. Li, and F. C. Lee, "A three phase CLLC converter with improved planar integrated transformer for fast charger applications," in *Proc. IEEE 4th Int. Conf. DC Microgrids*, 2021, pp. 1–5, doi: 10.1109/ICDCM50975.2021.9504644.

[21] C. Fei, Y. Yang, Q. Li, and F. C. Lee, "Shielding technique for planar matrix transformers to suppress common-mode EMI noise and improve efficiency," *IEEE Trans. Ind. Electron.*, vol. 65, no. 2, pp. 1263–1272, Feb. 2018, doi: 10.1109/TIE.2017.2733473.

Rimon Gadelrab (Student Member, IEEE) was born in Alexandria, Egypt, in 1990. He received the B.S. and M.S. degrees in electrical engineering from the Alexandria University, Alexandria, Egypt, in 2012 and 2015, respectively. He is currently working toward the Ph.D. degree with the Center for Power Electronics Systems, Virginia Tech, Blacksburg, VA, USA.

His current research interests include high frequency, high power density, and high-efficiency power conversion.

Fred C. Lee (Life Fellow, IEEE) received the B.S. degree from the National Cheng Kung University, Tainan City, Taiwan, in 1968, and the M.S. and Ph.D. degrees from the Duke University, Durham, NC, USA, in 1972 and 1974, respectively, all in electrical engineering.

He is a University Distinguished Professor Emeritus with Virginia Polytechnic Institute and State University (Virginia Tech), Blacksburg, VA, USA, and the Founder and Director Emeritus of the Center for Power Electronics Systems, an engineering research center consisting of 80 corporations. The mission of the center is "to provide leadership through global collaboration to create electric power processing systems of the highest value to society." He holds 105 U.S. patents and has authored or coauthored more than 335 journal articles and more than 780 refereed technical papers. During his tenure with Virginia Tech, he has supervised to completion 88 Ph.D. and 93 master's students. His research interests include high-frequency power conversion, magnetics and EMI, distributed power systems, renewable energy, power quality, high-density electronics packaging and integration, and modeling and control.

Dr. Lee is a recipient of the William E. Newell Power Electronics Award in 1989; PCIM Award for Leadership in Power Electronics Education presented at HFPC in 1990; the Arthur E. Fury Award for Leadership and Innovation in1998; the Honorary Sun Yuen Chuan Chair Professor of National Tsing Hua University in Taiwan in 2001; the Ernst-Blickle Award sponsored by SEW-EURODRIVE Foundation in 2005; the Distinguished Alumni Award from National Cheng Kung University in 2006; the Honorary Li Kwoh-Ting Chair Professor of National Cheng Kung University in 2011; Inaugural Member of the Virginia Tech Entrepreneur Hall of Fame in 2012; Honorary Chair Professor of National Chiao Tung University in Taiwan in 2014; Honorary Chair Professor of Tsinghua University in China in 2017; and Honorary Professor of Huazhong University of Science and Technology in China in 2018. He was the President of the IEEE Power Electronics Society (1992–1994). He is a Member of the U.S. National Academy of Engineering, an Academician of the Academia Sinica in Taiwan, and a Foreign Member of the Chinese Academy of Engineering in the People's Republic of China. He is also a recipient of the IEEEMedal in Power Engineering in 2015 "for contributions to power electronics, especially high-frequency power conversion," and the Power Supply Technology Outstanding Achievement Award from China Power Supply Society (CPSS) in 2017. He was elected as National Academy of Inventors (NAI) Fellow in 2018, and endorsed in 2019 as a Leader in engineering and education with the Albert Nelson Marquis Lifetime Achievement Award.